# IMPACT OF THE CHIMNEY JUNCTION RADIUS ON THE AIRFLOW CHARACTERISTICS INSIDE A SOLAR CHIMNEY POWER PLANT

***Haythem NASRAOUI[1], Hani BENGUESMIA[2,*], Badis BAKRI[3], ZiedDRISS[1], Hedi KCHAOU[1]***

[1] Laboratory of Electro-Mechanic Systems (LASEM), National School of Engineers of Sfax (ENIS), University of Sfax (US), B.P. 1173, km 3.5 Soukra, 3038 Sfax, TUNISIA

[*2] Electrical Engineering Laboratory (LGE), University of M'sila, M'sila, Algeria.

[3] Department of Electrical Engineering, Faculty of Technology, University of M'sila, M'sila, Algeria

[4] Department of Mechanical Engineering, faculty of technology, M'sila University, M'sila, Algeria.

[*]Corresponding author; E-mail: hani.benguesmia@univ-msila.dz

*The chimney junction of Solar Chimney Power Plant (SCPP) was the main element coupled the solar collector to the chimney. It presents an important impact on the SCPP design, which is change the airflow direction. The numerical code "ANSYS Fluent" was used in this study to investigate how the chimney Junction radius affected the local airflow characteristics and the turbine site. Using test results from an experimental prototype constructed in Sfax, Tunisia, the numerical method was validated and verified. For four setups with various chimney connection radii, thermodynamic variables such as distributions of the total pressure, static temperature, static pressure, and magnitude velocity were examined. Also, the influence of these parameters on the air turbulence was analyzed through the transition zone. The results showed that the local airflow characteristics and therefore the SCPP efficiency were significantly impacted by changes in junction radius. Besides, the maximum velocity inside the chimney was varied and changes its location when the junction radius changed. These facts affect directly the overall turbine expenditure, which represented in terms of structure and power capacity.*

Key words*: Renewable energy, solar chimney power plant, junction radius, turbulent airflow.*

## 1. Introduction

The excessive use of fossil fuels and the rise in pollution rates drive people to look for renewable resources. Among these resources, solar thermal technologies are efficient a system harnesses the heat from the sun to produce electricity. Specifically, SCPP is a mean of power generation from the solar energy. The few chemicals produced by the solar chimney power plant are one of its key advantages. It comprises four mainly parts which are the collector, the chimney, the turbine and the transition element. The transition element is an important zone, considered of the location of the flow direction change. It is typically consisting of the chimney junction and the guide

wall. A schematic of the SCPP compositions is shown in figure 1. Under the transparent collector roof, the SCPP system is based on both the greenhouse effect and natural convection. The solar radiation absorbed by the ground (absorber) is converted into heat energy and emitted again to the collector roof. In fact, the air receives both the energy types liberated by the ground. When the air is heated, its density is decreases. In order to produce a pressure difference between the chimney's input and output, airflow is then created inside the chimney. The hot air is moved and raised at the tower to turn a turbine that is coupled with an electric generator [1]. Schlaich constructed the first pilot prototype in Manzanraes Spain, which generated 50 kW of electricity power [2]. The power output and the efficiency of the SCPP were depends mainly on its geometrical and environmental parameters. The performance of the SCPP is directly impacted by external factors such as sun radiation and ambient temperature, which the operator cannot change. Only, it has a good agreement in the hot climate [3]. Frederick et al. [4] pointed out the critical roles of the climatic conditions in enhancing the power output. In this field, several experimental prototypes were built and tested over the worldwide [5-9]. Kasaeian et al. [10] presented an experimental investigation of the whether effects on the SCPP efficiency based on a small prototype built in Iran. Mostafa et al. [11] examined the impact of Saudi Arabia weather conditions. A triangular solar chimney was created and put up on a home's roof by Al-Kayiem et al. [12].They investigated the effects of the shape of the solar collector's inlet and emphasized how it impacts the solar chimney's effectiveness. The study of the form and the size of the different SCPP elements is a primary step to designing the solar chimney power plant. Haaf et al. [2, 13] implied that the chimney height and the temperature rise in the collector are leading factors for to determine the power output. Li et al. [14] provided a complete model for resolving the thermal balance equations in the collector in order to study the effect of the collecting radius on the SCPP potential. The findings revealed that while the potential typically improves with increasing collector radius, there is a limit radius where the potential trend slows down. By computing the temperature profile along the chimney, Zhou et al. [15] also calculated the power output. There is a maximum chimney height where the air temperature is consistent, according to the authors. The impact of the collector roof height with a horizontal wall on the flow behavior inside the SCPP was investigated by Ayadi et al. [16]. The authors noted that a tall collector might have an adverse effect on the SCPP system's thermodynamic efficiency. Ayadi et al. [17] shown in a different piece of study that a solar collector with a negative slope is more effective than a horizontal collector. A diverging SCPP was the subject of a numerical analysis by Hu et al. [18] in several scales. A number of numerical simulations were studied at by Bouabidi et al. [19] to analyze the SCPP with various chimney configurations. Based on the optimal turbine placement and the maximum velocity at the chimney, they showed that the diverging chimney is the best scenario among all the possibilities they investigated at. Backstrom and Gannon [20] inferred that diffusor chimney for the solar chimney power plant can be decreased the kinetic energy loss and thus enhance the SCPP efficiency. A diverging SCPP design with variable opening chimney angles was reported by Patel et al. in [21]. They discovered that the rise in divergent chimney angles could not considerably enhance power output. Moreover, many studies examined the transition part of the solar chimney power plant. Bernardes[22] developed a theoretical analysis describing the laminar convection in SCPP to enhance the geometrical parameters. He focused on the shape of the collector to chimney zone and the guide wall. Ming et al. [23] investigated the parameters of thermodynamic flow in the transition zone with and without a guide wall. They discovered that the inclusion of these components makes it possible to alter air velocity by 18%, improving SCPP

performance. Hu et al. [24] analyzed the effect of the guide wall design on the SCPP efficiency based on small-scale prototype. They developed varies simulations with the same junction radius but they changed the height and the radius of the guide wall. These works have been fixed the junction radius in all configurations. Despite this interest, no one to the best of our knowledge studied the chimney junction radius and its impact on the thermodynamic characteristics of the SCPP. The objective of this paper is to establish out how the turbulent airflow within a solar chimney power plant is impacted by the chimney junction radius. Using the commercial program "ANSYS Fluent," the thermodynamic and turbulence characteristics are supplied for a number of settings. With the same chimney and collector dimensions, four-junction radius is investigated. The benefit of using the CFD method is expected to its accuracy and high capacity. A prototype constructed in Tunisia serves as the basis for an experimental validation to regulate the numerical method's efficiency.

Specifically, the objectives can be outlined as follows; evaluate the Influence of Chimney Junction Radius, examine Turbine Site and Airflow Characteristics and Contribute to Renewable Energy Knowledge.

## 2. Methodology

### 2.1. Experimental prototype

In order to verify the airflow behavior inside a solar chimney, an experimental test is required. Figs 1 and 2 illustrates a SCPP prototype that is being created at the national engineering school of Sfax (ENIS) in southern Tunisia. The collector, absorber, chimney, and chimney support make up its four components. Due to its high solar radiation transmissivity, a polyethylene film was taken into consideration as the collector material. Convective exchange under the collector is increased by putting a rubber absorber made of black rubber on the sol. The black rubber is distinguished by its significant emissivity and absorptivity, which are 0.92 and 0.95, respectively. A steel framework that has been placed in the soil serves as the chimney and is made of PVC pipe. PVC is distinguished by its low weight and resistance to environmental factors like wind and temperature. Table 1 shows the dimensions of the prototype. The collector has the dimensions $H_c$=0.1 m in height and $D_c$=3.7 m in diameter. The PVC pipe has the dimensions $H_{ch}$=2.9 m in height and $D_{ch}$=0.16 m in diameter.

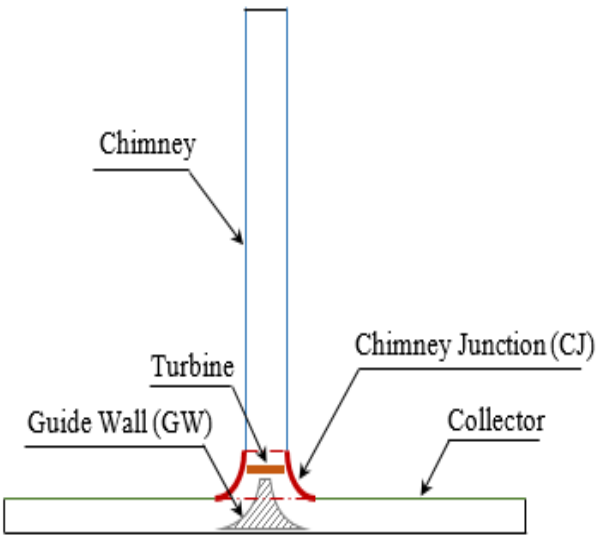


**Figure 1.** SCPP compounds

**Figure 2.** Prototype of the solar chimney

**Table 1.** Prototype dimensions

| Component | Height (m) | Diameter (m) | Thickness (mm) |
|---|---|---|---|
| Chimney | 2.95 | 0.16 | 4 |
| Collector | 0.1 | 3.7 | 1 |
| Absorber | - | 3.7 | 3 |

### 2.2. Mathematical model

Using the commercial code "ANSYS Fluent version 17.0," two-dimensional steady numerical simulations are created to examine how the junction radius affects the local airflow characteristics. The energy equation and Navier-Stokes equations are the governing equations that describe the airflow inside the solar chimney.

Navier-Stokes equations' momentum equations (2 and 3) and continuity equation (1) are shown in the cylindrical coordinate as follows:

$$\frac{\partial \rho}{\partial t} + \frac{1}{r}\frac{\partial}{\partial z}(r\rho u) + \frac{\partial}{\partial z}(\rho w) = 0 \tag{1}$$

$$\frac{\partial(\rho u)}{\partial t} + \frac{1}{r}\frac{\partial(\rho u u)}{\partial r} + \frac{\partial(\rho V w)}{\partial z} = -\frac{\partial p}{\partial r} + \frac{1}{r}\frac{\partial}{\partial r}\left(\mu r \frac{d(u)}{dr}\right) + \frac{\partial}{\partial z}\left(\mu \frac{d(u)}{dz}\right) - 2\mu\left(\frac{u}{r^2}\right) \tag{2}$$

$$\frac{\partial(\rho w)}{\partial t} + \frac{1}{r}\frac{\partial(\rho u w)}{\partial r} + \frac{\partial(\rho V w)}{\partial z} = -\frac{\partial p}{\partial z} + \frac{1}{r}\frac{\partial}{\partial r}\left(\mu r \frac{d(w)}{dr}\right) + \frac{\partial}{\partial z}\left(\mu \frac{d(w)}{dz}\right) - (\rho_0 - \rho)g \tag{3}$$

As seen below, the energy equation is written:

$$\frac{\partial(\rho T)}{\partial t} + \frac{1}{r}\frac{\partial(r\rho u T)}{\partial r} + \frac{\partial(\rho V T)}{\partial z} = \frac{1}{r}\frac{\partial}{\partial r}\left(r\frac{\lambda}{c_p}\frac{\partial(T)}{\partial r}\right) + \frac{\partial}{\partial z}\left(\frac{\lambda}{c_p}\frac{\partial(T)}{\partial z}\right) \tag{4}$$

The typical k-ε turbulence model is used to represent the airflow turbulence brought on by the buoyancy force inside the solar chimney. Two transport equations that define this model are the turbulent kinetic energy k and its dissipation rate ε.

The following is how the turbulent kinetic energy equation is written:

$$\begin{aligned}\frac{\partial}{\partial t}(\rho k) + \frac{1}{r}\frac{\partial}{\partial r}(r\rho u k) + \frac{\partial}{\partial z}(\rho w k) = \frac{1}{r}\frac{\partial}{\partial r}\left(r\left(\mu + \frac{\mu_t}{\sigma_k}\right)\frac{\partial}{\partial r}(k)\right) + \\ \frac{\partial}{\partial z}\left(\left(\mu + \frac{\mu_t}{\sigma_k}\right)\frac{\partial}{\partial z}(k)\right) + G_k + \frac{\beta g \mu_t}{Pr_{kt}}\frac{\partial}{\partial z}(k) - \rho\varepsilon\end{aligned} \tag{5}$$

The following is how the dissipation rate equation is expressed:

$$\begin{aligned}\frac{\partial}{\partial t}(\rho\varepsilon) + \frac{1}{r}\frac{\partial}{\partial r}(r\rho u\varepsilon) + \frac{\partial}{\partial z}(\rho w\varepsilon) \\ = \frac{1}{r}\frac{\partial}{\partial r}\left(\left(r\mu\frac{\mu_t}{\sigma_\varepsilon}\right)\frac{\partial}{\partial r}(\varepsilon)\right) + \frac{\partial}{\partial z}\left(\left(\mu + \frac{\mu_t}{\sigma_k}\right)\frac{\partial}{\partial z}(\varepsilon)\right) - G_k C_{1\varepsilon}\rho\frac{\varepsilon}{k} - C_{2\varepsilon}\rho\frac{\varepsilon^2}{k}\end{aligned} \tag{6}$$

Where $\mu_t$is the turbulent viscosity presented in equation 8, the turbulent kinetic energy's k and dissipation rate's ε values are in charge of controlling the situation immediately.

$$\mu_t = \rho C_\mu \frac{k^2}{\varepsilon} \tag{7}$$

Experimentally developed constant numbers$C_{1\varepsilon}$, $C_{2\varepsilon}$and $C_\mu$ are used here. $C_{1\varepsilon}$=1.44, $C_{2\varepsilon}$=1.92 and $C_\mu$=0.09. The amount of turbulent kinetic energy (kg.m$^{-1}$.s$^{-3}$) produced by mean velocity gradients is known as $G_k$. The turbulent Prandtl numbers and for k are, correspondingly and are equal to $\sigma_k$=1 and $\sigma_\varepsilon$=1.3.

There are several simplifying assumptions needed to model the SCPP.

- The subject is axi-symmetric and two-dimensional,
- The low Mach number makes the fluid incompressible,
- There is very little heat flow (negligible) caused by viscous heat dissipation,
- The air density variation caused by a temperature gradient is modeled using the Boussinesq approximation.

$$\rho = \rho_0[1 - \beta(T - T_0)] \tag{8}$$

Where is the air's thermal expansion coefficient, $\rho_0$ and $\beta$are the reference densities, respectively. To calculate the incident solar irradiation on the collector wall, it is determined to utilize the discrete ordinate model (DO). The following equations provide the output of the DO model:

The total intensity is calculated by adding the spectral intensities throughout the wavelength bands.

$$I(\vec{r}, \vec{s}) = \sum_k I_{\lambda_k}(\vec{r}, \vec{s})\Delta\lambda_k \tag{9}$$

$$\nabla.(I_\lambda(\vec{r}, \vec{s})\vec{s}) + (a_\lambda + \sigma_s)I_\lambda(\vec{r}, \vec{s}) = a_\lambda n^2 I_{b\lambda} + \frac{\sigma_s}{4\pi}\int_0^{4\pi} I_\lambda(\vec{r}, \vec{s}')\Phi(\vec{s}, \vec{s}')\, d\Omega' \tag{10}$$

When the wavelength is λ, the scattering coefficient is $\sigma_s$, the spectral absorption coefficient is $\alpha_\lambda$, and the black body intensity is $I_{b\lambda}$, respectively.

The Finite Volume Method is used to numerically solve the current mathematical model (FVM). All discretization parameters are applied to the figure, known as upwind. The simple method achieves in resolving the pressure-velocity relationship. For all residuals values, the convergence criterion is fixed at $10^{-6}$ in order to minimize simulation error.

### 2.3. Computational domains

To analyze how the local airflow characteristics are affected by the chimney connection radius, four configurations with different junction radius, $R_J$=0 m, $R_J$=0,05 m, $R_J$=0,1 m and $R_J$=0,2 m are carried out. Figure 3 shows the different considered configurations. The first one is analogous to the test prototype. However, the other configurations are giving by varied junction radius.

The chimney height ($H_{ch}$), collector height ($H_c$), and collector diameter ($D_c$) are always equal to 2.9 m, 0.1 m, and 3.7 m, respectively.

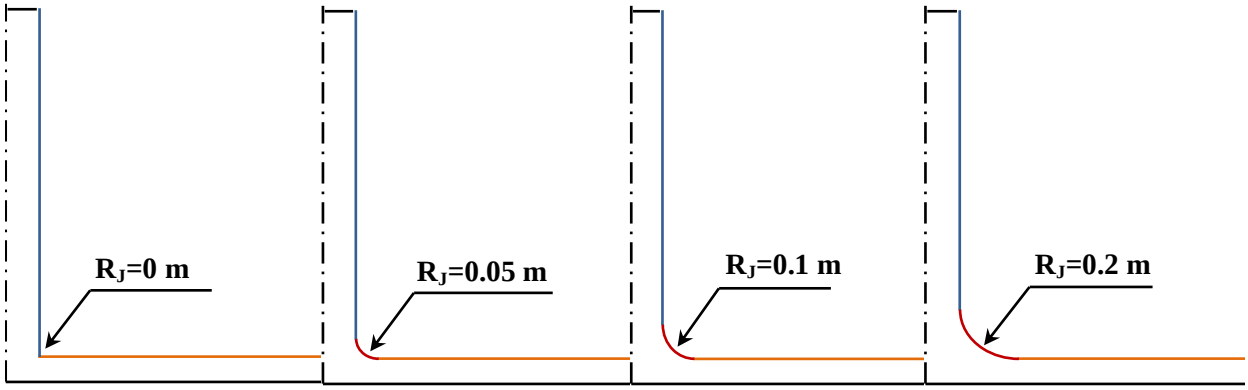


**Figure 3.** Proposed configurations

### 2.4. Bouandry conditions

Figure 4 illustrates the imposed boundary conditions. The collector roof is characterized as a semi-transparent wall by using the DO radiation model. The absorber, connection, and chimney are all considered opaque walls. Convection and radiation heat transfer modes are used on the absorber and collector walls for the thermal boundary conditions.

These conditions revealed the air heating process by greenhouse effect. This type of boundary condition is named “mixed”. However, the other walls are taken as adiabatic walls.

The working requirements were determined using experimental data collected on August 2nd, 2017, at 13:00. The various sun irradiation values and its anticipated beam direction are displayed in Table 2 at 13:00.

| | |
|---|---|
| Collector inlet | p = 101325 [Pa]<br>$T_0$ = 308 [K] |
| Chimney outlet | p = 101325[ Pa] |
| Collector wall | h = 8 [$W.K^{-1}.m^{-2}$]<br>$T_0$ = 308 [K] |
| Chimney wall | Q = 0 [$W.m^{-2}$] |
| Absorber wall | h = 8 [$W.K^{-1}.m^{-2}$]<br>$T_0$ = 308 K] |

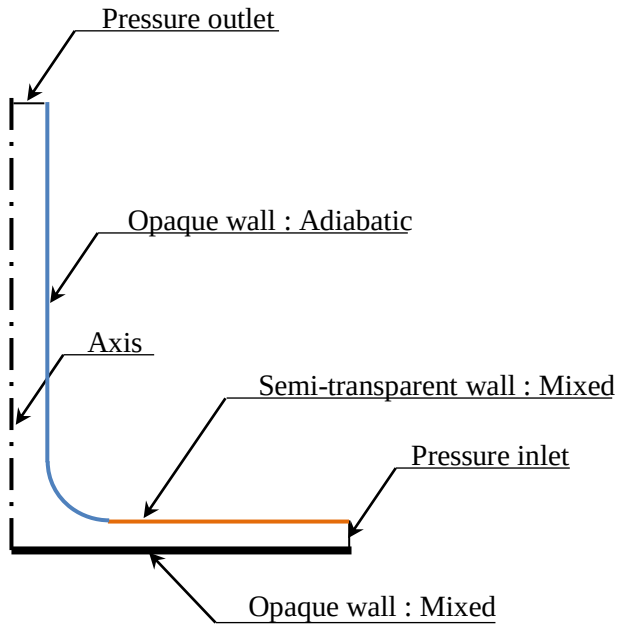


**Figure 4.** Boundary conditions

**Table 2**. Radiations components

| | | |
|---|---|---|
| **Solar irradiation** | Direct | 880 |
| | Diffuse | 83.3 |
| **Beam direction** | Chimney axis | 0.946 |
| | Collector axis | 0.152 |

## 3. Meshing effect and validation

An essential process in simulation, mesh creation (or meshing), directly influences model convergence and analysis accuracy. This study uses structural quadrature cells to mesh the SCPP's 2D axisymmetric domain. The regions that are close to walls have a gradual transition from the walls to the inside of the domain. This technique can improve the stability of the volume control under the collector's heat transfer problem. An overview of the applied meshing to the design with a junction radius of $R_J$=0.2 m is shown in Figure 5. The ideal element count was determined via a grid independence test, and several meshing configurations are investigated to shorten the meshing time. The meshing effect is examined using the built-in prototype's dimensions. Figure 6 compares the experimental and numerical temperature profiles along the collector centerline for the example under investigation. These findings make it obvious that the recommended numerical value, when compared to the experimental data for the three various cell numbers, is statistically significant. As a result, the third mesh defined by 20647 is selected as the best one. After meshing optimization, it is believed that the most efficient numerical model will be a useful tool for analyzing the impacts of suggested designs in a solar power plant chimney flow.

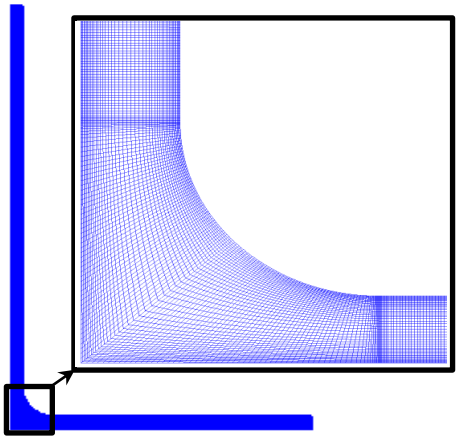

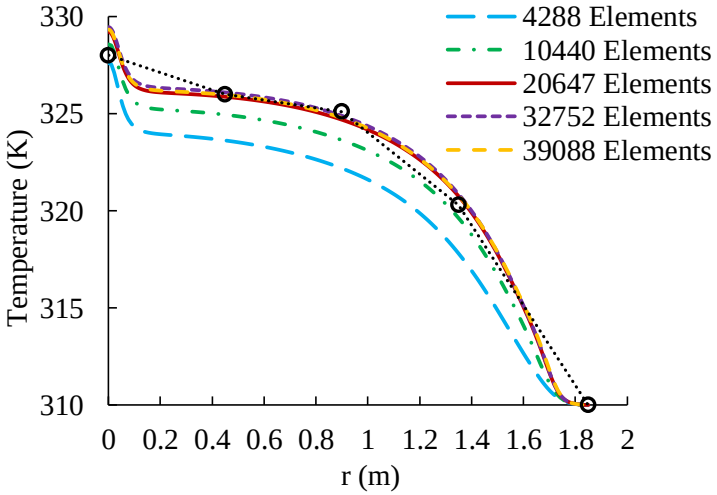


**Figure 5.** Meshing grid**Figure 6.** Meshing effect

## 4. Resultsnand discussion

### 4.1. Air flow through the transition element

The junction shape presents an important effect on air behavior when the direction of the flow changes. The transition zone for the four junction radii under consideration is shown in figure 7 as

having variations in turbulent kinetic energy, velocity, static pressure, and its rate of dissipation; $R_J$=0 m, $R_J$=0,05 m, $R_J$=0,1 m and $R_J$=0,2 m. Our findings show that the airflow across the transition zone is affected in all respects by a change in junction radius. In one hand, the couple pressure-velocity presents a peak value for all cases. From one configuration to another, this peak's value fluctuates. In reality, a significant acceleration zone appears in the first case. The non-junction chimney has a significant depression zone at the chimney entrance that is inversely proportional to the velocity. Moreover, these peak values dropped with the increase of the junction radius. The velocity curve has approximately a linear tendency in the cases with large radius, while the static pressure decreases gradually along the junction. It can be describing these facts by the venturi effect at the chimney inlet. Indeed, an increase of the junction radius make more smoothly upward of the airflow into the chimney. In other hand, both the turbulence characteristics k and ε are directly affected by the change of the junction radius. In fact, it is evident that the kinetic energy of the turbulent flow and its rate of dissipation present the high values in the SCPP without chimney junction. Moreover, because of the low friction factor in the case of a high connection radius, the rate of turbulent kinetic energy dissipation is insignificant.

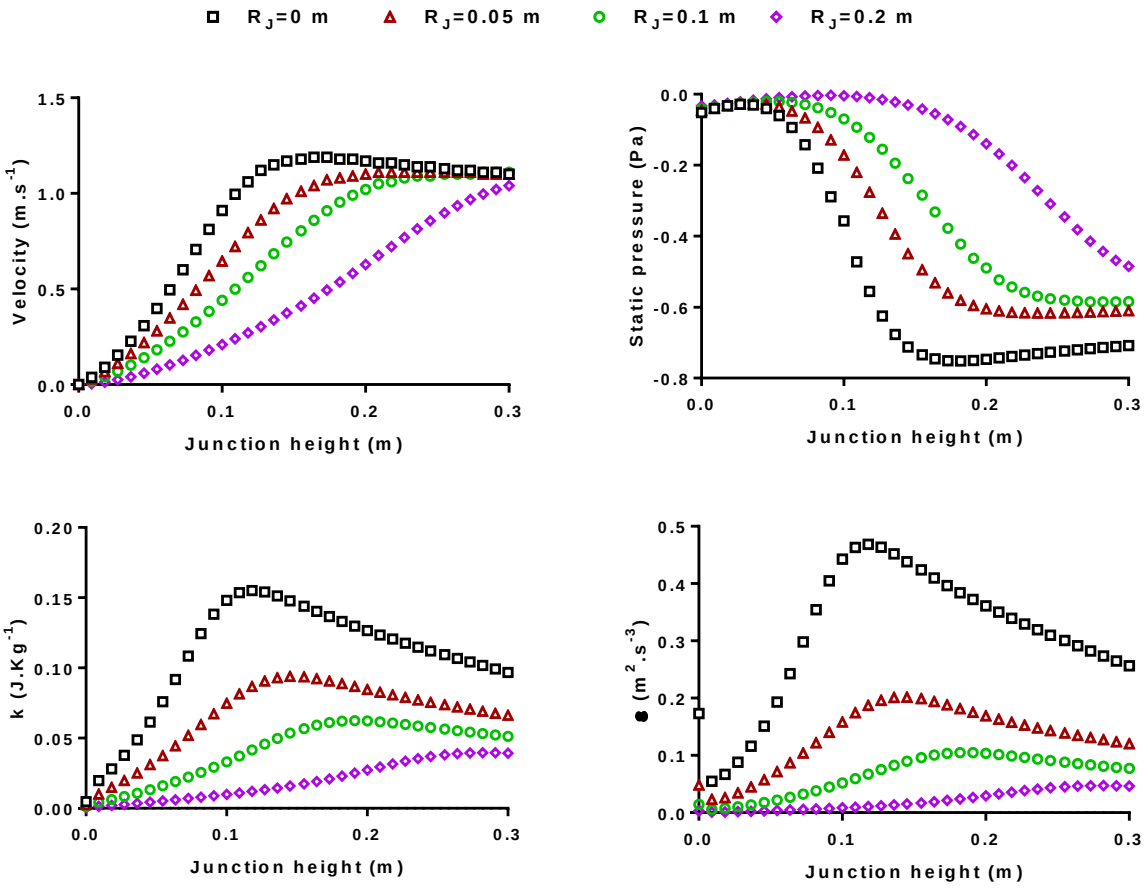


**Figure 7.** Local characteristics profiles through the transition element

### 4.2. Temperature

The temperature distributions in the solar chimney's axisymmetric plane for various connection radii, $R_J$=0 m, $R_J$=0,05 m, $R_J$=0,1 m and $R_J$=0,2 m are shown in figure 8. These findings demonstrate

that the temperature distribution is slightly impacted by a change in junction radius. At the SCPP input, the temperature is always equal to $T_0$=310 K, the ambient temperature. The gradient between the collector output and intake then becomes rather large. Due to the adiabatic planned chimney and the low height, the airflow in the chimney region continues to be hot. Otherwise, the temperature features significant values near the absorber wall which is closely equal to T=331K for all considered configurations. This fact may be explained by considering how the chimney connection only affects the dynamic properties inside the SCPP system.

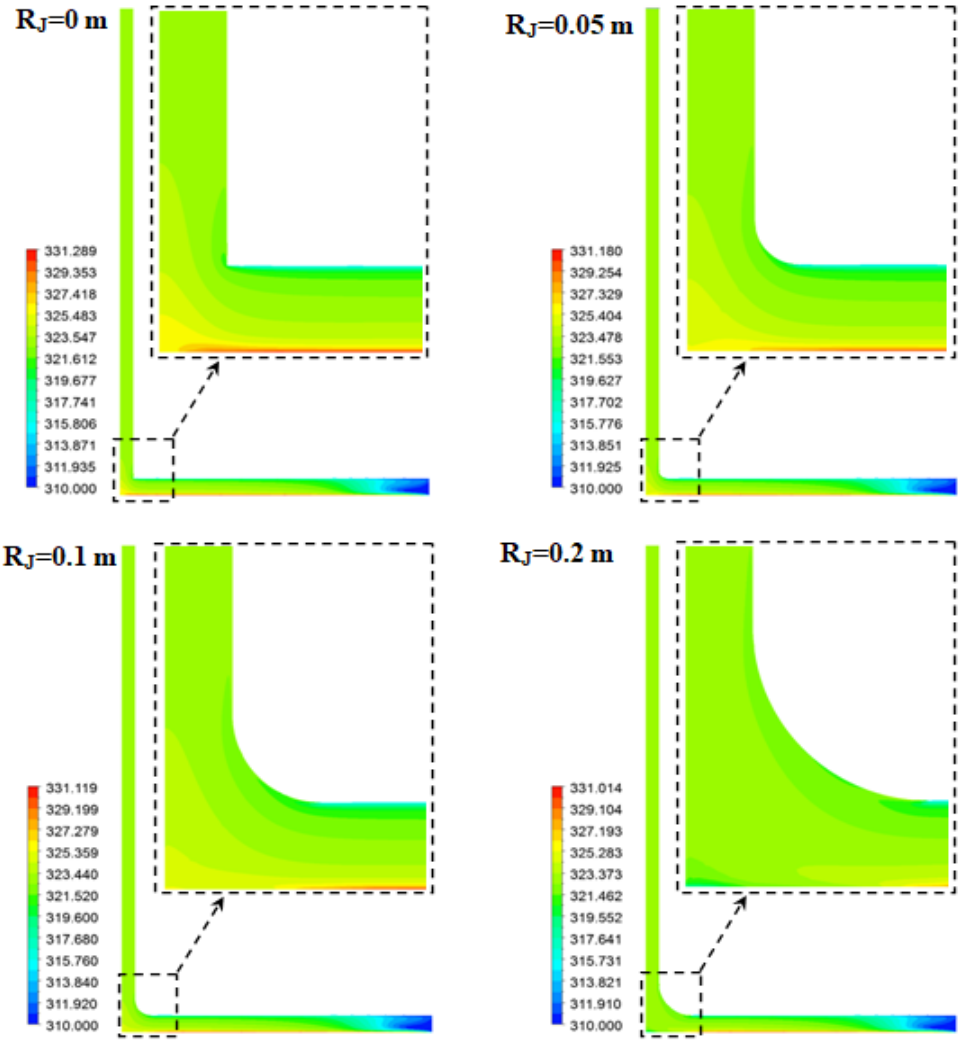


**Figure 8.** Temperature distribution

### 4.3. Magnitude velocity

The magnitude velocity distributions for various connection radii in the solar chimney's axisymmetric plane, $R_J$=0 m, $R_J$=0.05 m, $R_J$=0.1 m and $R_J$=0.2 m are shown in figure 9. From these results, it can be seen that the change of the junction radius affects the magnitude velocity in distributions and values. In practice, for the typical chimney arrangement, the acceleration zone is near the chimney inlet ($R_J$=0 m), while the air velocity accelerates at the chimney outlet in the configurations with junction element. The magnitude velocity in the first case increased constantly from the collector inlet to the SCPP center, and then peaked at 1.189 m.s$^{-1}$ at inlet of the chimney. The

magnitude velocity first decreased above the chimney intake before leveling out and remaining constant along the chimney. For the three other configurations, the air velocity presents the same behavior with the standard solar chimney in the collector, while a gradual rise in the magnitude velocity appears from the junction element to the chimney exit. Indeed, it is clear that the peak zone is modified when increasing the junction radius.

Meanwhile, as a result of the decrease in friction loss in the transition zone, the junction radius grows together with the magnitude velocity's maximum value. These conditions result in it being equivalent to V=1,189 $m.s^{-1}$ in the first instance, V=1,248 $m.s^{-1}$ in the second, V=1,277 $m.s^{-1}$ in the third, and V=1,298 $m.s^{-1}$ in the fourth case.

Figure 10 shows the bar charts of the maximum and the inlet average values in the chimney for the four junction radii. Overall, the maximum velocity experienced an upward trend, while the overall value at the chimney inlet is fell and rose throughout the junction radius range. Although, the maximum and the average velocity for $R_J$=0 m are almost equals. The magnitude velocity's maximum value for the three junction radius, $R_J$=0,05 m, $R_J$=0,1 m and $R_J$=0,2 m, is higher than the one of first case. With the solar chimney with a junction element, however, the values at the chimney entrance are incredibly low. Figure 9 supports these observations.

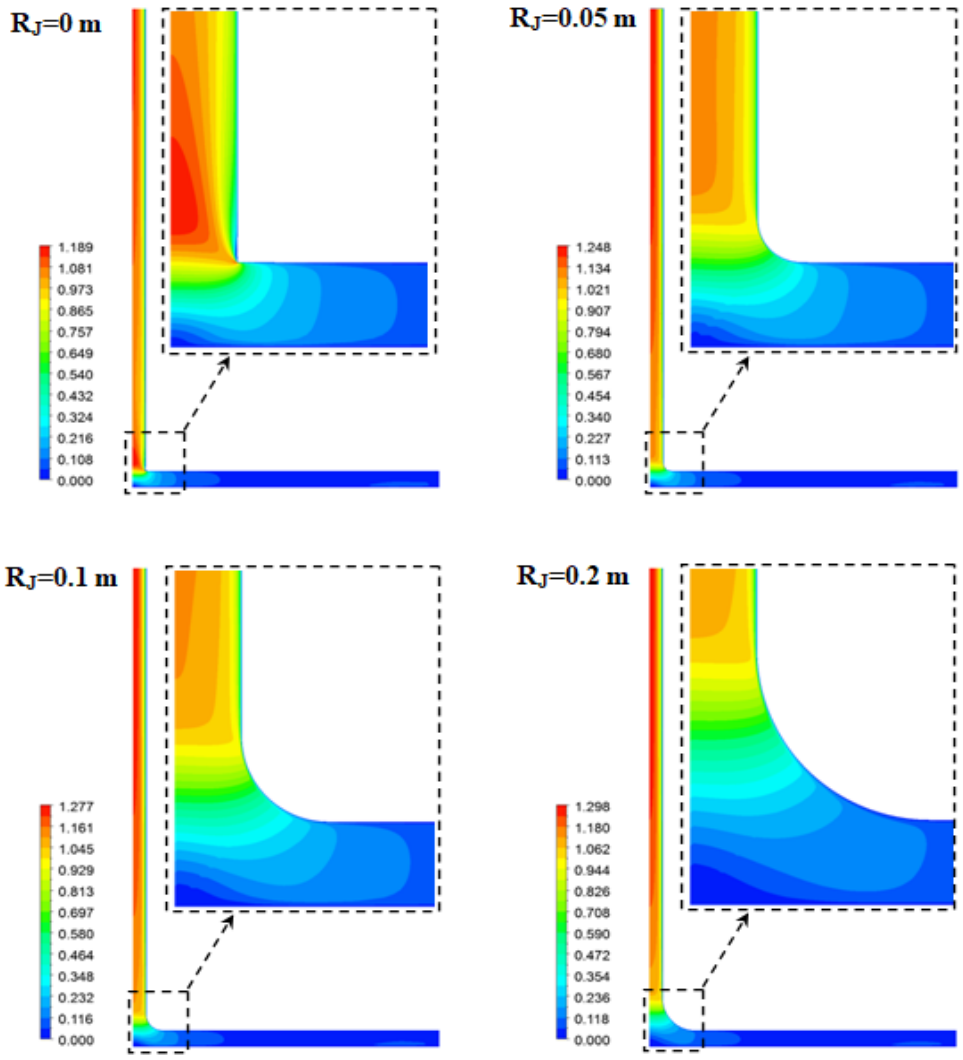


**Figure 9.** Magnitude velocity distribution

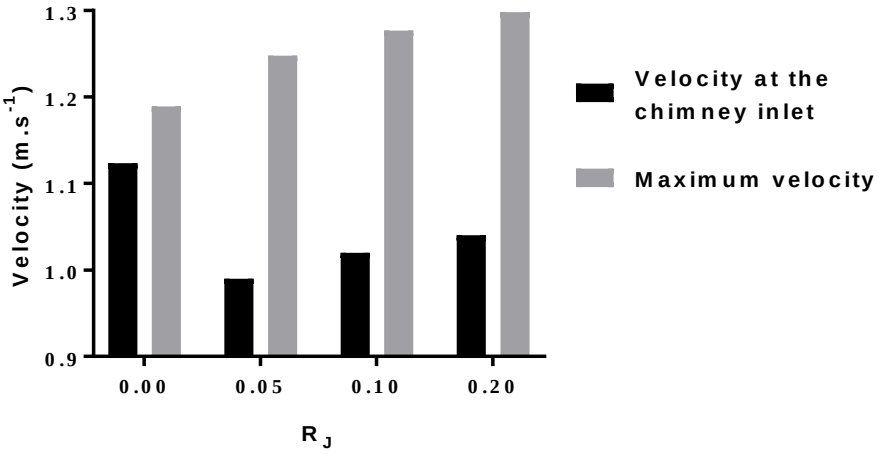


**Figure 10.** Magnitude velocity

### 4.4. Pressure

The static pressure distributions at various connection radii in the solar chimney's axisymmetric plane, $R_J$=0 m, $R_J$=0,05 m, $R_J$=0,1 m and $R_J$=0,2 m are shown in figure 11.

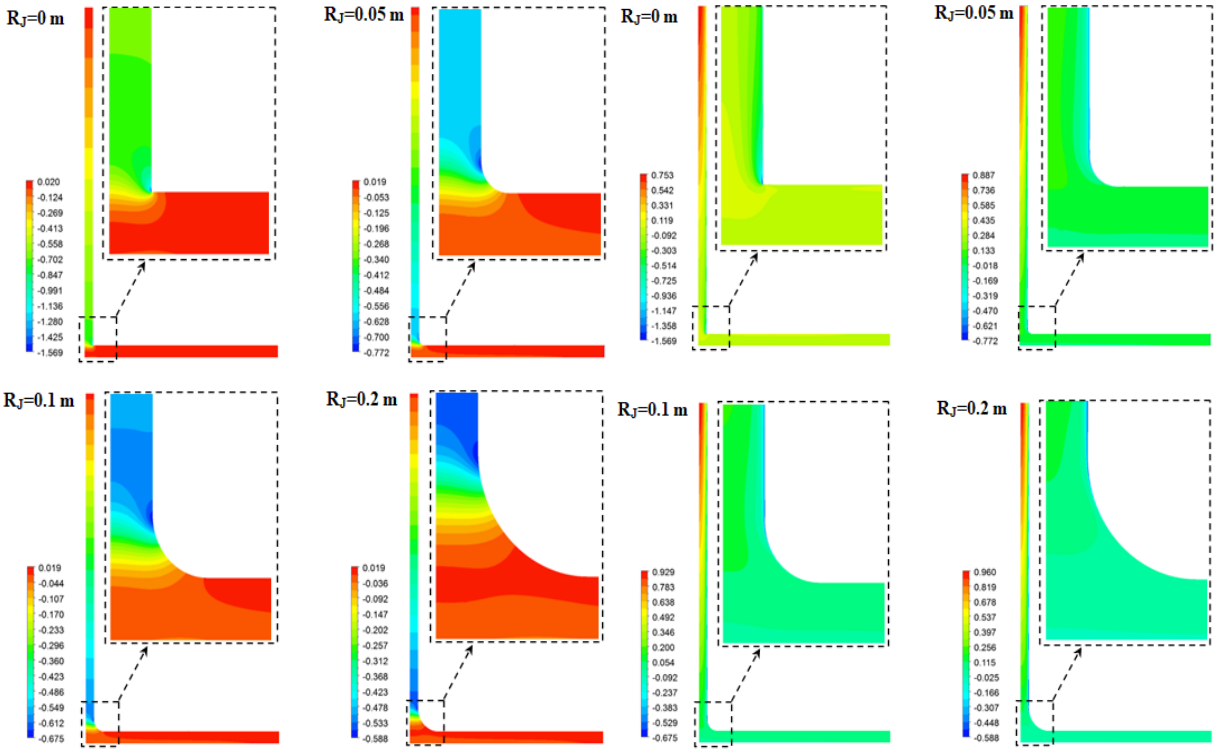


**Figure 11.** Static pressure distribution**Figure 12.** Total pressure distribution

According to these results, the static pressure distribution differs from one configuration to another, much as the magnitude velocity distribution. However, the static pressure under the collector is kept rather constant, and only a modest reduction is visible at the collector outlet. The static pressure plummets steeply throughout the transition section when the air changes it. Then, a gradual rise along the chimney is shown to reach the ambient pressure at the chimney outlet. It is clear that the depression zone upsurges with the increase of the junction radius. The small depression area is shown in the first configuration, while a large area appears in the fourth configuration. In fact, the chimney

junction could make an enlargement in the depression zone, which presents a good agreement for turbine power. However, the lowest value of the relative static pressure increases with the increase of the junction radius. In these conditions, it is equal to p=-1,569 Pa for the first case, p=-0,772 Pa for the second case, p=-0,675Pa for the third case and p=-0.588 Pa for the fourth case. This fact is confirmed by the results shown in figure 7. The total pressure is the sum of the static and the dynamic pressures. The pressure extracted by the turbine is a part of the total pressure at the turbine location. Indeed, the total pressure is an informative parameter for the turbine energy input. Figure 12 depicts the static pressure distribution for each of the four analyzed configurations in the solar chimney's axisymmetric plane.

The static pressure depicts the same distribution form in every situation, as is seen from this image. As it progresses through the chimney, it rises gradually until it reaches the ambient pressure at the chimney exit. It is essentially constant inside the collector. The weakest numbers illustrate how the four instances differ.

### 4.5. Turbulent kinetic energy

Figure 13 displays the turbulent kinetic energy distributions for each of the four configurations under consideration in the axisymmetric plane of the SCPP system.

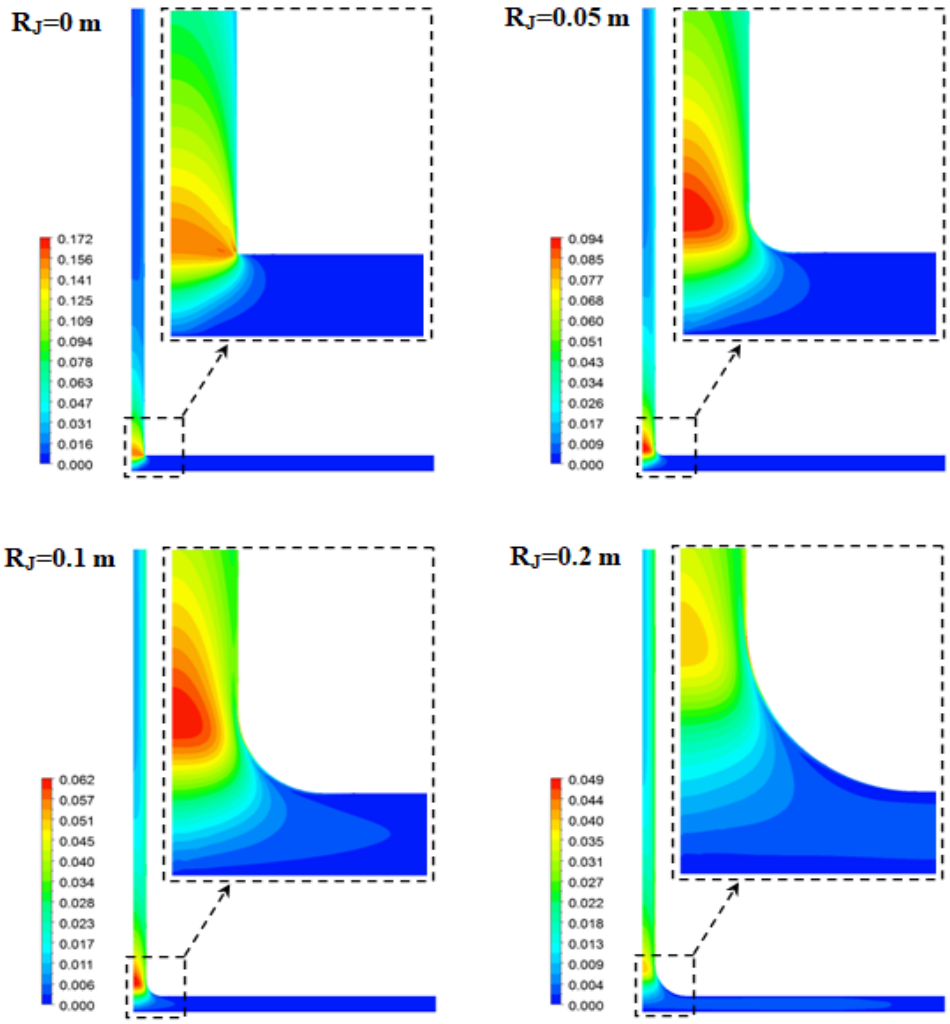


**Figure 13.** Distribution of the turbulent kinetic energy..

These results make it abundantly evident that altering the junction radius causes a change in the turbulent kinetic energy distribution. For all cases, the turbulent kinetic energy presents low values under the collector. After then, a brusque growth starts to occur in the transition zone, and it progressively fades away along the chimney pipe. Only at the collector-chimney transition zone does each of the four variants differ from one another. For the configuration without junction radius, the turbulent kinetic energy looks very weak at the chimney inlet. However, the high turbulent intensity zone presents a large distribution for the other configurations. The increase of the junction radius is decreases the maximum value of the turbulent kinetic energy. In these conditions, it is equal to k=0,172 $m^2.s^{-2}$ for the first case, k=0,094 $m^2.s^{-2}$ for the second case, k=0,062 $m^2.s^{-2}$ for the third case and k =0,049 $m^2.s^{-2}$ for the fourth case.

### 4.6. Turbulent viscosity

Figure 14 depicts the turbulent viscosity distributions for the various connection radii under consideration in the solar chimney's axisymmetric plane.

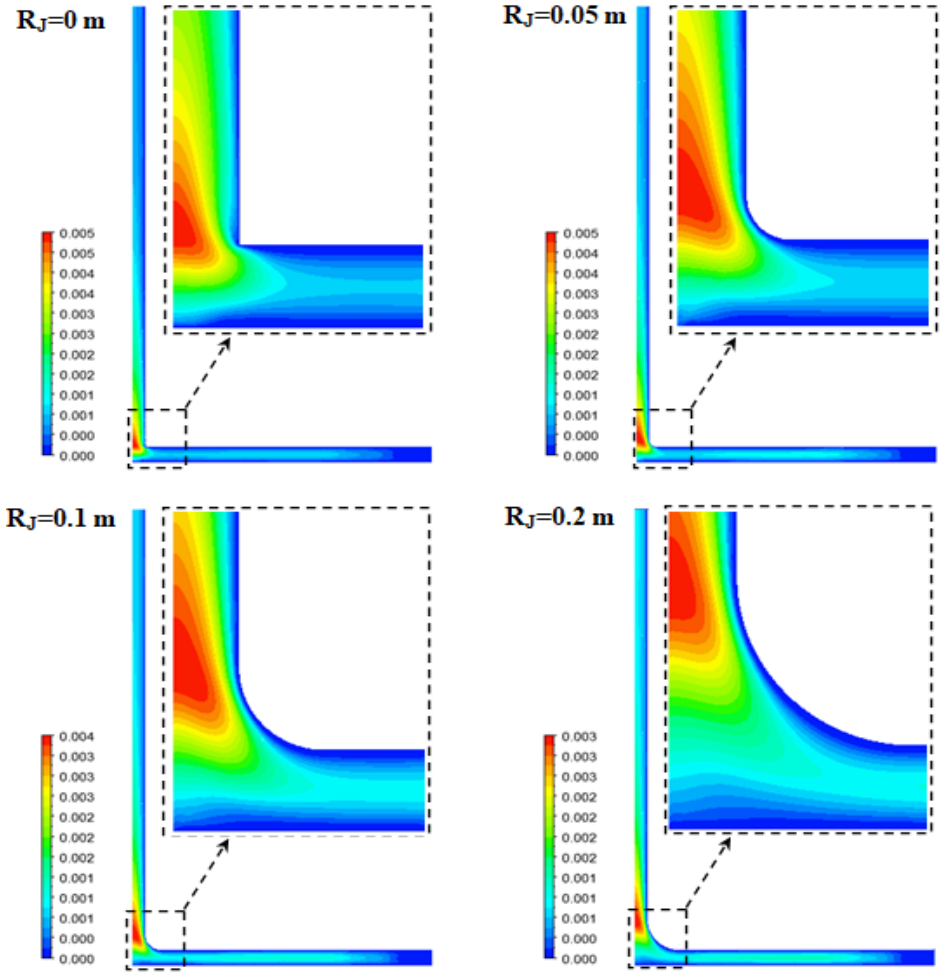


**Figure 14.** Distribution of the turbulent viscosity.

These results indicate that the turbulent viscosity has the same distribution form in each of the four configurations. It is smoothly varying in the collector and the chimney regions then the highest values appear at the chimney inlet. However, the maximum turbulent viscosity value is slightly

decreased with the increase of the junction radius. In these conditions, it is equal to $\mu_t$=5,$10^{-3}$ kg.$m^{-1}$.$s^{-1}$ for the first case, $\mu_t$=5,$10^{-3}$ kg.$m^{-1}$.$s^{-1}$ for the second case, $\mu_t$=4,$10^{-3}$ kg.$m^{-1}$.$s^{-1}$ for the third case and $\mu_t$=3,$10^{-3}$ kg.$m^{-1}$.$s^{-1}$ for the fourth case.

## 5. Conclusion

The performance of the SCPP is investigated in this study in relation to the junction radius. Analysis of the four junction radius local airflow characteristics; $R_J$=0 m, $R_J$=0,05 m, $R_J$=0,1 m and $R_J$=0,2 m. The used numerical model was validated with our experimental results, which are taken on $2^{sd}$ August 2017. The findings showed that:

Advantageously, the maximum velocity values are localized at the chimney inlet for the small junction radius which present a benefit solution to install the turbine near the ground. A negligible dissipation rate of the turbulent kinetic energy was appeared for the largest junction radius. This fact presents a small energy loss disadvantageously, the maximum velocity values are localized at the chimney top for the largest junction radius. In fact, the turbine installation required more energy and more operation cost.

From this study, the solar chimney power plant has been mentioned without junction part has a good agreement in terms of structure and operation cost. However, the SCPP with typical junction presents an efficient device in terms of energetic efficiency.

Field Application: In practical terms, understanding how the chimney junction radius affects airflow is crucial for optimizing the design and performance of SCPPs in real-world settings. The observed changes in local airflow characteristics have direct implications for turbine site selection, structure design, and power capacity. For instance, a specific chimney junction radius may result in more efficient airflow distribution within the chimney, positively impacting turbine performance and, subsequently, power generation. This knowledge is pivotal for engineers and designers working on SCPP projects, providing them with insights to make informed decisions about chimney design parameters.

**Recommendations for future research**

Explore the influence of ambient wind conditions on the performance of the solar chimney. Understand how wind patterns interact with the chimney and collector to optimize efficiency and minimize potential challenges.

Conduct a comprehensive economic viability assessment of SCPPs with varying chimney junction radii. Consider factors such as initial costs, maintenance, and long-term operational expenses to provide a holistic view of the technology's feasibility.

Investigate the use of advanced numerical modeling techniques beyond ANSYS Fluent, considering emerging technologies or methodologies that may provide more accurate predictions of airflow dynamics and system performance.

Explore the potential benefits of integrating SCPPs with wind turbine systems in hybrid configurations. Investigate how the synergy between solar and wind energy can enhance overall renewable energy generation.

Conduct a comprehensive environmental impact assessment of SCPPs with a focus on the chosen chimney junction radius. Consider factors such as land use, wildlife impact, and emissions to ensure sustainable development.

Collaborate with industry partners to implement SCPPs with optimized chimney junction radii in real-world settings. Monitor and evaluate performance over an extended period to validate theoretical findings and gather practical insights.

These recommendations aim to enhance the current work and suggest exciting avenues for future research in the field of Solar Chimney Power Plants.

**Nomenclatures**

| **Symbols** | | **Greek symbols** | |
|---|---|---|---|
| $c_p$ | Air's specific thermal capacity [$J.kg^{-1}K^{-1}$ ] | β | Thermalexpansion coefficient [-] |
| $D_{ch}$ | Diameter of a chimney [m] | ε | Turbulent kinetic energy dissipation rate [$m^2.s^{-3}$] |
| $D_c$ | Diameter of the collector [m] | μ | Dynamic viscosity [$m^2.s^{-1}$] |
| e | Thickness [mm] | ρ | Density of the air [$Kg.m^{-3}$] |
| g | Acceleration due to gravity [$m.s^{-2}$] | | |
| $H_c$ | height of the collector [m] | | |
| $H_{ch}$ | Height of the chimney [m] | | |
| I | Global radiation [$W.m^{-2}$] | | |
| k | Turbulent kinetic energy [$m^2.s^{-2}$] | | |
| P | Pressure [Pa] | | |
| Pr | Prandtl number [-] | | |
| r | Radial coordinate [m] | | |
| $R_J$ | Junction radius [m] | | |
| t | Time [s] | | |
| T | Temperature [K] | | |
| u | Radial-direction velocity [-] | | |
| V | Air velocity [$m.s^{-1}$] | | |
| w | Tangentially directed velocity [$m.s^{-1}$] | | |
| z | Axial coordinate [m] | | |

**References**


[1] Schlaich, J.,*The solar chimney: electricity from the sun*, Edition Axel Menges, 1995.

[2] Haaf,W., *et al.*, Solar chimneys part I: principle and construction of the pilot plant in Manzanares. *International Journal of Solar Energy*, 2 (1983), pp.3-20.

[3] Nizetic,S., *et al.*, Analysis and feasibility of implementing solar chimney power plants in the Mediterranean region,*Energy*, 33 (2008),pp. 1680-1690.

[4] Onyango,F.N., *et al.*, The potential of solar chimney for application in rural areas of developing countries,*Fuel*, 85 (2006) pp. 2561-2566.

[5] Kasaeian,A., *et al.*, A review on solar chimney systems,*Renewable and Sustainable Energy Reviews*, 67 (2017),pp. 954-987.

[6] Jemli,M.R., *et al.*, Experimental investigation of solar tower with chimney effect installed in CRTEn, Tunisia,*International Journal of Hydrogen Energy*, 42 (2017), pp. 8650-8660.

[7] Kalash,S.,*et al.*, Experimental investigation of the solar collector temperature field of a sloped solar updraft power plant prototype,*Solar Energy*. 98 (2013),pp. 70-77.
[8] Ghalamchi, M.,*et al.*, An experimental study on the thermal performance of a solar chimney with different dimensional parameters. *Renewable Energy*, 91 (2016), pp.477-483.
[9] Faisal, S. H., *et al.*, Hydrodynamic study of a solar chimney power plant for better power production. Thermal Science, 00 (2023), pp. 42-42.https://doi.org/10.2298/TSCI220819042F
[10] Kasaeian,A., *et al.*, Experimental investigation of climatic effects on the efficiency of a solar chimney pilot power plant,*Renewable and Sustainable Energy Reviews*, 15, (2011), pp. 5202-5206.
[11] Abdelmohimen,M.A., *et al.*, Numerical investigation of solar chimney power plants performance for Saudi Arabia weather conditions,*Sustainable Cities and Society*, 38, (2018),pp. 1-8.
[12] Al-Kayiem,H.H., *et al.*, Experimental and numerical analysis of the influence of inlet configuration on the performance of a roof top solar chimney,*Energy and Buildings*, 159, (2018),pp. 89-98.
[13] Haaf,W., Solar chimneys: part ii: preliminary test results from the Manzanares pilot plant,*International Journal of Sustainable Energy*, 2, (1984),pp.141-161.
[14] Li,J.-y., *et al.*, Effects of collector radius and chimney height on power output of a solar chimney power plant with turbines,*Renewable energy*, 47 (2012),pp.21-28.
[15] Zhou,X., *et al.*, Analysis of chimney height for solar chimney power plant,*Applied Thermal Engineering*, 29 (2009),pp. 178-185.
[16] Ayadi,A., *et al.*,Experimental and numerical analysis of the collector roof height effect on the solar chimney performance,*Renewable Energy*., 115 (2017), pp. 649-662.
[17] Ayadi,A., *et al.*, Experimental and numerical study of the impact of the collector roof inclination on the performance of a solar chimney power plant,*Energy and Buildings*, 139 (2017),pp. 263-276.
[18] Hu,S., *et al.*,Impact of the geometry of divergent chimneys on the power output of a solar chimney power plant,*Energy*, 120 (2017) pp. 1-11.
[19] Bouabidi,A., *et al.*, Study of solar chimney in Tunisia: Effect of the chimney configurations on the local flow characteristics,*Energy and Buildings*,169 (2018), pp.27-38.
[20] von BackströmT.W., *et al.*, Compressible flow through solar power plant chimneys. *Journal of Solar Energy Engineering*, 122(2000),pp.138-145.
[21] Patel,S.K., *et al.*,Computational studies on the effect of geometric parameters on the performance of a solar chimney power plant,*Energy Conversion and Management*, 77 (2014) pp. 424-431.
[22] dos Santos Bernardes,M.A., Numerical analysis of natural laminar convection in a radial solar heater,*International journal of thermal sciences*, 38 (1999), pp. 42-50.
[23] Tingzhen,M.,*et al.*, Analytical and numerical investigation of the solar chimney power plant systems,*International Journal of Energy Research*, 30 (2006),pp. 861-873.
[24] Hu, S.,*et al.*, Chan. Effect of guide wall on the potential of a solar chimney power plant,*Renewable Energy*, 96 (2016), pp. 209-219.

Submitted: 5.08.2023.
Revised: 2.02.2024.
Accepted: 18.02.2024.